A&A 593, A96 (2016)
DOI: 10.1051/0004-6361/201628808

Astronomy & Astrophysics

Searching for supergiant fast X-ray transients with *Swift*

P. Romano[1], E. Bozzo[2], P. Esposito[3], B. Sbarufatti[4,5], F. Haberl[6], G. Ponti[6], P. D'Avanzo[4], L. Ducci[7,2], A. Segreto[1], C. Jin[6], N. Masetti[8,9], M. Del Santo[1], S. Campana[4], and V. Mangano[5]

[1] INAF, Istituto di Astrofisica Spaziale e Fisica Cosmica – Palermo, via U. La Malfa 153, 90146 Palermo, Italy
e-mail: romano@ifc.inaf.it
[2] ISDC Data Center for Astrophysics, Université de Genève, 16 chemin d'Écogia, 1290 Versoix, Switzerland
[3] Anton Pannekoek Institute, University of Amsterdam, Postbus 94249, 1090 GE Amsterdam, The Netherlands
[4] INAF, Osservatorio Astronomico di Brera, via E. Bianchi 46, 23807 Merate, Italy
[5] Department of Astronomy and Astrophysics, Pennsylvania State University, University Park, PA 16802, USA
[6] Max-Planck-Institut für extraterrestrische Physik, Giessenbachstraße, 85748 Garching, Germany
[7] Institut für Astronomie und Astrophysik, Eberhard Karls Universität, Sand 1, 72076 Tübingen, Germany
[8] INAF, Istituto di Astrofisica Spaziale e Fisica Cosmica – Bologna, via Gobetti, 101, 40129 Bologna, Italy
[9] Departamento de Ciencias Físicas, Universidad Andrés Bello, Fernández Concha 700, Las Condes, Santiago, Chile

Received 28 April 2016 / Accepted 18 June 2016

ABSTRACT

Supergiant fast X-ray transients (SFXTs) are high mass X-ray binaries (HMXBs) hosting a neutron star and an OB supergiant companion. We examine the available *Swift* data, as well as other new or archival/serendipitous data, on three sources: IGR J17407−2808, 2XMM J185114.3−000004, and IGR J18175−2419, whose X-ray characteristics qualify them as candidate SFXT, to explore their properties and test whether they are consistent with an SFXT nature. Since IGR J17407−2808 and 2XMM J185114.3−000004 triggered the Burst Alert Telescope on board *Swift*, the *Swift* data enable us to provide their first arcsecond localisations, leading to an unequivocal identification of the source CXOU J174042.0−280724 as the soft X-ray counterpart of IGR J17407−2808, as well as their first broadband spectra, which can be fit with models generally describing accreting neutron stars in HMXBs. While still lacking optical spectroscopy to assess the spectral type of the companion, we propose 2XMM J185114.3−000004 as a very strong SFXT candidate. The nature of IGR J17407−2808 remains, instead, more uncertain. Its broadband properties cannot exclude the fact that the emission originates from either an HMXB (and in that case, an SFXT) or, more likely, a low-mass X-ray binary. Finally, based on the deep non-detection in our XRT monitoring campaign and a careful reanalysis of the original INTEGRAL data in which the discovery of the source was first reported, we show that IGR J18175−2419 is likely a spurious detection.

Key words. X-rays: binaries – X-rays: individuals: IGR J17407–2808 – X-rays: individuals: 2XMM J185114.3–000004 – X-rays: individuals: IGR J18175–2419

1. Introduction

Supergiant fast X-ray transients (SFXTs) are high mass X-ray binaries (HMXBs) hosting most likely a neutron star (NS) and an OB supergiant companion (Sguera et al. 2005; Negueruela et al. 2006). Unlike normal supergiant HMXBs, which display a fairly constant average luminosity with typical variations by a factor of 10−50 on time scales of a few hundred to thousands of seconds, SFXTs are characterised by hard X-ray flares reaching, for a few hours, 10^{36}–10^{37} erg s^{-1} (see Romano et al. 2014b, for a catalogue of hard X-ray flares). SFXTs have also been found to be significantly subluminous with respect to classical supergiant HMXBs like Vela X-1 (Lutovinov et al. 2013; Bozzo et al. 2015), and show a soft X-ray dynamical range of up to six orders of magnitude (Sguera et al. 2005; Romano et al. 2015), since their luminosities can be as low as $\sim 10^{32}$ erg s^{-1} during quiescence (e.g. in't Zand 2005; Bozzo et al. 2010). The origin of this different behaviour is still unknown (see, e.g. Bozzo et al. 2013, 2015) and thus the different models proposed to explain the behaviour for these sources are still being debated. The models include a combination of more pronounced dense inhomogeneities (clumps) in the winds of the SFXT supergiant companions compared to those of classical systems (in't Zand 2005; Walter & Zurita Heras 2007; Negueruela et al. 2008), magnetic/centrifugal gates generated by the slower rotational velocities and higher magnetic fields of the NSs hosted in SFXTs (Grebenev & Sunyaev 2007; Bozzo et al. 2008, 2016), or a subsonic settling accretion regime combined with magnetic reconnections between the NS and the supergiant stellar field transported by its wind (Shakura et al. 2014, and references therein).

Most SFXTs were first discovered, or classified as such, based on their hard X-ray properties (e.g. Sguera et al. 2005; Negueruela et al. 2006; Walter et al. 2015) as observed by INTEGRAL/IBIS (Ubertini et al. 2003). Subsequently, their long-term behaviour has also been extensively investigated (see Romano et al. 2014b) with other coded-mask large field-of-view instruments, such as the *Swift*/Burst Alert Telescope (BAT, Barthelmy et al. 2005). These hard X-ray monitors, however, share similiar sensitivity limits, which enable them to catch only the brightest portion of any transient event. Owing to their transient nature, SFXTs are indeed particularly difficult to find unless they experience frequent and relatively bright flares. A legitimate question is, therefore, whether we have already discovered the majority of Galactic SFXTs.

In a recent work, Ducci et al. (2014) address the issue of how common the SFXT phenomenon is, and conclude that, since detection of the entire population is hindered by the SFXT's peculiar transient properties, a fraction of the population is probably yet to be identified, and that we are likely missing SFXTs with low outburst rates or large distances.

Ducci et al. (2014), considered two datasets, the 100-month *Swift*/BAT catalogue (Romano et al. 2014b) and the first nine years of INTEGRAL/ISGRI data (Paizis & Sidoli 2014), applied two distinct statistical approaches to derive the expected number of SFXTs emitting bright flares in the Milky Way, $N \approx 37^{+53}_{-22}$. This value not only agrees with the expected number of HMXBs in the Galaxy derived from high-mass binary evolution studies (van den Heuvel 2012; Dalton & Sarazin 1995, and references therein), but also suggests that SFXTs constitute a sizeable fraction of X-ray binaries with supergiant companions. The SFXT class currently includes a mere dozen confirmed individuals, that is, X-ray binaries for which optical/IR spectroscopy has firmly established the presence of a supergiant primary of O or B spectral type (e.g. Romano et al. 2014b; Romano 2015). About as many candidate SFXTs are known, for which no optical spectroscopy has been obtained until now, but which have a reported history of bright, large dynamic range hard X-ray flaring. Since we expect a larger number of SFXTs in the Galaxy, it is worthwhile to increase the sample of these sources through new and archival multifrequency data studies of SFXT candidates and other promising unclassified transients. A larger sample of SFXTs would ultimately allow us to gain more information to understand the accretion mechanisms responsible for their enigmatic behaviour.

The *Swift* SFXT Project (Romano 2015) has been investigating the X-ray properties of the SFXTs since 2007, exploiting the unique observing capabilities of *Swift* (Gehrels et al. 2004). In particular, we have been performing follow-up observations of several tens of SFXT outbursts caught by the BAT (Romano et al. 2011b; Farinelli et al. 2012; Romano et al. 2015, and references therein), with the X-ray Telescope (XRT, Burrows et al. 2005) and the UV/Optical Telescope (UVOT, Roming et al. 2005), and have carried out long-term monitorings of virtually all SFXTs, also including five classical systems for comparison purposes. *Swift* broadband data of bright flares are particularly useful for increasing the SFXT sample, since they enable us to make a solid connection between the hard X-ray transient and its soft X-ray counterpart. As the XRT positional accuracy is as good as a few arcseconds, this type of association allows us to identify, in most cases, the optical/IR source associated with the X-ray transient and, subsequently, schedule dedicated optical spectroscopic campaigns to unveil its nature.

In this paper, we present the newly collected XRT and UVOT monitoring data of the three sources 2XMM J185114.3−000004, IGR J17407−2808, and IGR J18175−2419, which showed an X-ray activity reminiscent of what is typically observed from the SFXTs during either the BAT triggers or the follow-up observations in the soft X-rays. Our main goal is to use the new data to investigate the associations of these systems with the SFXT class. We also supplement our data set by including: (i) serendipitous archival *XMM-Newton* observations of IGR J17407−2808; (ii) serendipitous archival *XMM-Newton* and ESO Very Large Telescope (VLT) observations of 2XMM J185114.3−000004; (iii) archival INTEGRAL observations of IGR J18175−2419 carried out with the IBIS/ISGRI instrument.

2. The sample

2XMM J185114.3−000004 is a source in the *XMM-Newton* XMMSSC catalogue (Watson et al. 2009; Lin et al. 2012) that triggered the BAT on 2012 June 17 (Barthelmy et al. 2012). At the time of discovery, the source showed an increase in the X-ray flux that was at least a factor of 40 compared to previous detections. Recently, Bamba et al. (2016) have analysed an ∼100 ks *Suzaku* observation of the supernova remnant (SNR) G32.8−0.1 that serendipitously included 2XMM J185114.3−000004 and found evidence of high time variability with flares on timescales of a few hundred seconds superimposed on a general decaying X-ray flux during the observation. No pulsations were found, but the flares were noticed as being spaced apart from one another by ∼7000 s. The 3−10 keV spectrum was characterised by a high absorption ($N_{\rm H} \sim 10^{23}$ cm^{-2}) and a photon index $\Gamma \sim 1.6$, with a 2−10 keV flux of $\sim 10^{-11}$ erg cm^{-2} s^{-1}.

IGR J17407−2808 was discovered with INTEGRAL as a new transient on 2004 Oct. 9 (Götz et al. 2004; Kretschmar et al. 2004) and associated with either SBM2001 10 (Sidoli et al. 2001) or the ROSAT source 2RXP J174040.9−280852. Based on its hard X-ray behaviour, Sguera et al. (2006) proposed it as a candidate SFXT since they noted peculiarly quick strong flares (20−60 keV, peak flux 800 mCrab) lasting a couple of minutes. Heinke et al. (2009) found a likely association with the soft X-ray source CXOU J174042.0−280724 (Tomsick et al. 2008). Following a BAT trigger on 2011 October 15, Romano et al. (2011a) identified CXOU J174042.0−280724 as the soft X-ray counterpart of IGR J17407−2808. This in turn led to the identification of the candidate IR counterpart (Greiss et al. 2011; Kaur et al. 2011). If confirmed, this could disprove the SFXT hypothesis, since the most likely optical companion seems at present to be a late type-F dwarf.

The transient IGR J18175−2419 was serendipitously discovered (Grebenev 2013) in the IBIS/ISGRI data of the INTEGRAL observations performed in the direction of the X-ray nova SWIFT J174510.8−2624 on 2012 September 26. The characteristic short (1 h) flare displayed by the source at discovery, combined with its spectrum described by a hard power law ($\Gamma \sim 2.1$) and a possible exponential cut-off above 80 keV, suggested that IGR J18175−2419 could be a newly discovered SFXT source. No further detections of the source have been reported to date.

3. Data reduction

The *Swift* and *XMM-Newton* observing logs for 2XMM J185114.3−000004, IGR J17407−2808, and IGR J18175−2419 are reported in Table 1−3, respectively. The VLT observation logs are in Table 4.

3.1. Swift

The *Swift* data were uniformly processed and analysed using the standard software (FTOOLS[1] v6.18), calibration (CALDB[2] 20160113), and methods. In particular, background-subtracted *Swift*/BAT light curves were created in the standard energy bands and mask-weighted spectra were extracted during the first orbit of the first automated target (AT) observation. We applied an energy-dependent systematic error vector to the BAT data. The *Swift*/XRT data were processed and filtered with the task XRTPIPELINE (v0.13.2). Pileup was corrected, when required, by adopting standard procedures (Vaughan et al. 2006; Romano et al. 2006). In these cases, the size of the point spread function (PSF) core affected by pile-up was determined by comparing the observed versus the nominal PSF, and excluding from the analysis all the events that fell within that region. In the case of 2XMM J185114.3−000004 (Table 1), we extracted source

[1] https://heasarc.gsfc.nasa.gov/ftools/ftools_menu.html
[2] https://heasarc.gsfc.nasa.gov/docs/heasarc/caldb/caldb_intro.html

Table 1. Log of X-ray observations of 2XMM J185114.3−000004 and spectral fit results.

Instrument	ObsID	Start time (UT)	End time (UT)	Exposure (s)	$N_{\rm H}$ ($\times10^{22}$ cm^{-2})	Γ	$F^a_{0.5-10\,\rm keV}$ (erg cm^{-2} s^{-1})	$F^a_{15-50\,\rm keV}$ (erg cm^{-2} s^{-1})	χ^2/d.o.f.
Swift/BAT evt	00524542000	2012-06-17 15:43:04	2012-06-17 17:58:19	1201	–	$2.6^{+0.4}_{-0.4}$	–	$(7.8\pm0.8)\times10^{-10}$	26.1/24
Swift/XRT WT	00524542000	2012-06-17 15:49:58	2012-06-17 17:14:58	17	[b]	[b]	$(3.4\pm0.7)\times10^{-10}$	–	–
Swift/XRT PC	00524542000	2012-06-17 15:50:11	2012-06-17 17:56:46	4305	14^{+4}_{-3}	$0.77^{+0.49}_{-0.44}$	$(1.1^{+0.5}_{-0.1})\times10^{-10}$	–	45.4/42
Swift/XRT PC	00524542001	2012-06-17 18:51:27	2012-06-18 01:39:58	5366	[b]	[b]	$(5.4\pm0.2)\times10^{-13}$	–	–
Swift/XRT PC	00524542002	2012-06-18 19:06:54	2012-06-18 19:33:56	1610	[b]	[b]	$<1.1\times10^{-12}$	–	3σ UL
Swift/XRT PC	00524542003	2012-06-18 22:09:31	2012-06-19 01:53:44	3831	[b]	[b]	$<1.3\times10^{-12}$	–	3σ UL
Swift/XRT PC	00524542004	2012-06-19 17:20:22	2012-06-19 17:36:57	985	[b]	[b]	$<1.6\times10^{-12}$	–	3σ UL
Swift/XRT PC	00524542005	2012-06-21 03:09:28	2012-06-21 03:26:59	1020	[b]	[b]	$<2.7\times10^{-12}$	–	3σ UL
Swift/XRT PC	00524542007	2012-06-23 04:47:40	2012-06-23 04:56:55	554	[b]	[b]	$<3.2\times10^{-12}$	–	3σ UL
Swift/XRT PC	00524542008	2012-06-24 03:48:15	2012-06-24 23:09:56	1158	[b]	[b]	$<1.8\times10^{-12}$	–	3σ UL
Swift/XRT PC	00524542009	2012-06-25 08:05:54	2012-06-25 22:38:56	1131	[b]	[b]	$(2.6\pm0.8)\times10^{-12}$	–	–
Swift/XRT PC	00524542010	2012-06-26 00:10:27	2012-06-26 00:25:55	923	[b]	[b]	$<2.5\times10^{-12}$	–	3σ UL
Swift/XRT PC	00524542011	2012-06-28 10:00:53	2012-06-28 10:17:56	1000	[b]	[b]	$<2.7\times10^{-12}$	–	3σ UL
Swift/XRT PC	00524542012	2012-06-29 06:55:10	2012-06-29 07:11:56	995	[b]	[b]	$<1.5<\times10^{-12}$	–	3σ UL
Swift/XRT PC	00524542013	2012-06-30 02:22:00	2012-06-30 02:38:55	1003	[b]	[b]	$<1.8<\times10^{-12}$	–	3σ UL
Swift/XRT PC	00524542014	2012-07-01 03:55:57	2012-07-01 03:59:55	228	[b]	[b]	$<6.7<\times10^{-12}$	–	3σ UL
Swift/XRT PC	00524542015	2012-07-02 03:48:53	2012-07-02 04:01:56	757	[b]	[b]	$<2.4<\times10^{-12}$	–	3σ UL
Swift/XRT PC	00524542016	2012-07-03 01:04:48	2012-07-03 02:26:54	1005	[b]	[b]	$<1.8<\times10^{-12}$	–	3σ UL
Swift/XRT PC	00524542017	2012-07-04 21:46:20	2012-07-04 22:01:55	923	[b]	[b]	$<1.9<\times10^{-12}$	–	3σ UL
Swift/XRT PC	00032512001	2012-08-08 01:19:37	2012-08-08 19:08:56	2745	[b]	[b]	$(5.1\pm0.7)\times10^{-12}$	–	–
Swift/XRT PC	00032512002	2012-08-11 10:43:32	2012-08-11 12:31:55	1464	[b]	[b]	$<1.9\times10^{-12}$	–	3σ UL
Swift/XRT PC	00032512004	2012-08-19 03:11:15	2012-08-19 06:31:55	3879	[b]	[b]	$<1.7\times10^{-12}$	–	3σ UL
Swift/XRT PC	00032512005	2012-08-31 15:02:03	2012-08-31 18:37:56	4719	[b]	[b]	$(3.4\pm0.4)\times10^{-12}$	–	–
Swift/XRT PC[c]	00044565001	2012-11-20 20:52:24	2012-11-20 21:00:56	506	[b]	[b]	$<1.8\times10^{-12}$	–	3σ UL
XMM Epic-pn[c]	0017740401	2003-10-05 00:53:54	2003-10-05 08:57:14	27 670	11 ± 5	1.6 ± 0.9	$(3.3^{+0.7}_{-0.4})\times10^{-13}$	–	45.2/42[e]
XMM Epic-MOS[c]	0017740401	2003-10-05 00:53:54	2003-10-05 08:57:14	27 670	13^{+6}_{-4}	$2.0^{+1.1}_{-0.9}$	$(5.0^{+1.5}_{-1.0})\times10^{-13}$	–	15.2/19[e]
XMM Epic-pn[c]	0017740501	2003-10-20 23:36:20	2003-10-21 07:56:20	28 667	6^{+12}_{-5}	$1.0^{+1.7}_{-1.3}$	$(1.5^{+0.8}_{-0.4})\times10^{-13}$	–	9.6/14[e]
XMM Epic-MOS[c]	0017740501	2003-10-20 23:36:20	2003-10-21 07:56:20	28 667	10^{+14}_{-6}	$1.2^{+2.0}_{-1.3}$	$(1.5^{+1.5}_{-0.8})\times10^{-13}$	–	8.4/7[e]
XMM Epic-pn[c]	0671510101	2012-03-18 09:44:36	2012-03-19 02:48:13	60 084	[d]	[d]	$<4\times10^{-15}$	–	3σ UL

Notes. The adopted spectral model for the fits is an absorbed power law. [(a)] Observed. [(b)] Adopting the same spectral parameters as in observation 0017740401 (pn). [(c)] Serendipitous observations. [(d)] Adopting the same spectral parameters as in observation 0017740501 (pn). [(e)] Cash statistics has been used during the fit.

events from annuli with inner/outer radii of 4/20 pixels (we note that for XRT, one pixel corresponds to 2.36″) during the first observation. In all other cases, a circle with a radius of 20 pixels was adopted. The background events were extracted from an annular region with an inner radius of 80 pixels and an external radius of 120 pixels centered at the source position. For IGR J17407−2808 (Table 2), the source events were extracted from annuli with inner/outer radii of 5/20 pixels in the first observation, and a circular region with a radius of 20 pixels in all other cases. Background events were extracted from annuli with inner/outer radii of 60/120 pixels centred at the source position. The XRT light curves were corrected for PSF losses and vignetting by using the XRTLCCORR tool and were background subtracted. In all observations, where no detection was achieved, the corresponding 3σ upper limit on the X-ray count rate was estimated by using the tasks SOSTA and UPLIMIT within XIMAGE (with the background calculated in the neighbourhood of the source position) and the Bayesian method for low-count experiments adapted from Kraft et al. (1991). For our spectral analysis, we extracted events in the same regions as those adopted to create the light curve; ancillary response files were generated with the task XRTMKARF to account for different extraction regions, vignetting, and PSF corrections.

The *Swift*/UVOT observed the targets simultaneously with the XRT. It used all filters during AT observations and with the "Filter of the Day", i.e. the filter chosen for all observations to be carried out during a specific day to minimize the filter-wheel usage, during all other observations. The data analysis was performed using the UVOTIMSUM and UVOTSOURCE tasks included in FTOOLS. The UVOTSOURCE task calculates the magnitude of the source through aperture photometry within a circular region centered on the best source position and applies the required corrections related to the specific detector characteristics. We adopted a circular region with a radius of 5″ for the photometry of the different sources. The background was evaluated in all cases by using circular regions with a radius of 10″.

3.2. XMM-Newton

The *XMM-Newton* EPIC-pn (Strüder et al. 2001) and EPIC-MOS (Turner et al. 2001) observations of 2XMM J185114.3−000004 and IGR J17407−2808 were processed by using the *XMM-Newton* Science Analysis Software (SAS, v. 15.0)[3].

2XMM J185114.3−000004 was serendipitously observed by *XMM-Newton* three times (see Table 1) on 2003 October 5 (ObsID 0017740401), on 2003 October 20 (ObsID 0017740501), and on 2012 March 18 (ObsID 0671510101). In all cases, the source was located at the very rim of the three EPIC cameras field of view (FOV). *XMM-Newton* observation data files (ODFs) for 2XMM J185114.3−000004 were processed to produce calibrated event lists using the standard *XMM-Newton* SAS. We used the EPPROC and EMPROC tasks to

[3] http://xmm.esac.esa.int/sas/

Table 2. Log of X-ray observations of IGR J17407−2808 and spectral fit results.

Instrument	ObsID	Start time (UT)	End time (UT)	Exposure (s)	$N_{\rm H}$ ($\times10^{22}$ cm^{-2})	Γ	$F^{a}_{0.5-10\,\rm keV}$ (erg cm^{-2} s^{-1})	$F^{a}_{15-50\,\rm keV}$ (erg cm^{-2} s^{-1})	χ^2/d.o.f.
Swift/BAT evt	00505516000	2011-10-15 01:13:06	2011-10-15 01:28:11	905	–	$1.3^{+0.5}_{-0.5}$	–	$(4.6\pm0.9)\times10^{-10}$	49.6/24
Swift/BAT evt (peak1)	00505516000	2011-10-15 01:12:26	2011-10-15 01:14:06	100	–	$2.1^{+0.6}_{-0.5}$	–	$(2.1\pm0.2)\times10^{-9}$	27.8/23
Swift/BAT evt (peak2)	00505516000	2011-10-15 01:27:04	2011-10-15 01:28:49	105	–	$1.9^{+0.4}_{-0.4}$	–	$(2.3\pm0.3)\times10^{-9}$	32.8/24
Swift/XRT PC	00505516000	2011-10-15 01:15:05	2011-10-15 03:03:32	772	$0.84^{+2.00\,b}_{-0.84}$	$-0.45^{+0.86}_{-0.71}$	$(6.8\pm0.9)\times10^{-11}$	–	68.9/68[c]
Swift/XRT PC	00036122001	2011-10-15 19:16:28	2011-10-15 20:27:37	983	[d]	[d]	$<2.1\times10^{-12}$	–	3σ UL
Swift/XRT PC	00036122002	2011-10-17 01:17:25	2011-10-17 01:34:01	988	[d]	[d]	$<2.1\times10^{-12}$	–	3σ UL
Swift/XRT PC	00036122003	2011-10-17 21:57:29	2011-10-17 22:14:05	980	[d]	[d]	$<2.7\times10^{-12}$	–	3σ UL
Swift/XRT PC	00036122004	2011-10-18 12:36:46	2011-10-18 12:53:57	1018	[d]	[d]	$<2.9\times10^{-12}$	–	3σ UL
Swift/XRT PC	00036122006	2011-10-20 12:47:59	2011-10-20 12:48:27	28	[d]	[d]	$<4.0\times10^{-11}$	–	3σ UL
Swift/XRT PC	00036122007	2011-10-21 14:26:20	2011-10-21 14:41:56	933	[d]	[d]	$<1.6\times10^{-12}$	–	3σ UL
Swift/XRT PC[e]	00032370001	2012-06-30 03:34:12	2012-06-30 03:43:56	584	[d]	[d]	$<4.5\times10^{-12}$	–	3σ UL
Swift/XRT PC[e]	00032370003	2012-07-12 11:09:06	2012-07-12 11:17:55	522	[d]	[d]	$<4.6\times10^{-12}$	–	3σ UL
Swift/XRT PC[e]	00032370004	2012-08-28 07:21:39	2012-08-28 07:29:56	484	[d]	[d]	$<2.3\times10^{-12}$	–	3σ UL
Swift/XRT PC[f]	All 3σ UL	2011-10-15 19:16:28	2012-08-28 07:29:56	6519	[d]	[d]	$<1.1\times10^{-12}$	–	3σ UL
XMM Epic-pn[e]	0764191301	2016-03-06 09:21:41	2016-03-06 19:34:01	30 678	$0.77^{+0.70}_{-0.47}$	$-0.11^{+0.28}_{-0.26}$	$(5.2^{+0.8}_{-0.3})\times10^{-13}$	–	29.6/19[g]
XMM Epic-MOS[e]	0764191301	2016-03-06 08:58:52	2016-03-06 19:38:06	35 923	–	–	–	–	–

Notes. A power-law was used to describe the BAT data, while an absorption component was included in the case of the XRT and *XMM-Newton* data. [(a)] Observed. [(b)] $N_{\rm H} < 5.1\times10^{22}$ cm^{-2} 3σ c.l. [(c)] Cash statistics. [(d)] Adopting the same spectral parameters as in observation 00505516000. [(e)] Serendipitous observations. [(f)] Combination of all data after T+10^4 s (from 00036122001 to 00032370004). [(g)] Simultaneous EPIC-pn and MOS1 fit.

Table 3. Log of X-ray observations of IGR J18175−241.

Instrument	ObsID	Start time (UT)	End time (UT)	Expo. (s)
Swift/XRT	00034136001	2016-03-06 12:41:58	2016-03-06 12:57:54	955
Swift/XRT	00034136002	2016-03-07 07:58:45	2016-03-07 08:16:53	1088
Swift/XRT	00034136003	2016-03-08 09:31:28	2016-03-08 09:47:53	963
Swift/XRT	00034136004	2016-03-09 00:03:16	2016-03-09 00:16:53	43
Swift/XRT	00034136005	2016-03-10 22:12:58	2016-03-10 22:27:56	888
Swift/XRT	00034136006	2016-03-11 14:05:57	2016-03-11 14:21:54	958
Swift/XRT	00034136007	2016-03-12 07:43:28	2016-03-12 07:59:54	985
Swift/XRT	00034136008	2016-03-13 01:04:33	2016-03-13 01:20:54	963
Swift/XRT	00034136009	2016-03-14 04:11:53	2016-03-14 04:27:53	20

Table 4. Optical data on 2XMM J185114.3−000004: VLT/NACO and *Swift*/UVOT observations.

Instrument	Time mid observation (UT)	Exposure (s)	Filter	Mag
VLT/NACO	2012-07-12 07:41:28	$5\times2\times60$ s	J	15.8 ± 0.1
VLT/NACO	2012-07-12 07:54:45	$5\times2\times60$ s	Ks	11.7 ± 0.1
Swift/UVOT	2012-06-26 06:57:11	8890	u	>21.84
Swift/UVOT	2012-06-17 16:49:25	533	b	>20.56
Swift/UVOT	2012-06-17 20:44:42	1834	v	>20.21
Swift/UVOT	2012-09-04 16:58:10	15 714	$m2$	>22.11
Swift/UVOT	2012-07-13 17:33:49	8589	$w1$	>21.79
Swift/UVOT	2012-06-24 09:58:43	4012	$w2$	>21.62

Notes. Magnitudes are in the Vega system and not corrected for Galactic extinction.

produce cleaned event files from the EPIC-pn and MOS cameras, respectively. EPIC-pn and EPIC-MOS event files were extracted in the 0.5−10 keV energy range and filtered to exclude high background time intervals. The obs. 0671510101 was moderately affected by flaring background episodes. The cleaned effective exposure time was of 40.8 ks. The obs. 0017740401 was not affected by a high background, and thus we retained for the following analysis the entire exposure time available (21.4 ks for the EPIC-pn and 27.4 ks for the two MOS). In obs. 0017740501, cleaning for the high-level background resulted in an effective exposure time of 17.9 ks for the EPIC-pn and 21.2 ks for the two MOS cameras. Source and background spectra were extracted by using regions in the same CCD.

IGR J17407−2808 was also observed serendipitously with *XMM-Newton* (see Table 2) on 2016 March 6 (ObsID: 0764191301, PI. G. Ponti) during a Galactic centre lobe scan performed as an extension of the *XMM-Newton* scan (Ponti et al. 2015a,b). The source was located at an off-axis angle of about 7.5 arcmin from the aim point of all EPIC cameras, which were operating in full-frame mode using the medium filter. We removed an interval of increased background flaring activity at the end of the observation, yielding an effective exposure of 34.9, 36.4, and 36.3 ks for the pn, MOS1, and MOS2, respectively. Unfortunately, the source was located right at the edge of CCD1 in both MOS cameras and only a small fraction of the point spread function was covered, leading to great uncertainties in the flux reconstruction. For the MOS2, the uncertainty was too large to be useful for any scientific analysis, and thus we discarded these data. The EPIC-pn and MOS1 energy spectra and time series of the source and the background were extracted from circular regions. The radii of these regions were chosen to maximize the signal-to-noise ratio (S/N) by using the SAS tasks EREGIONANALYSE and ESPECGET. We used single- and double-pixel events for the EPIC-pn camera and single- to quadruple-pixel events for the MOS1. For the energy spectra, events with FLAG ≠ 0 were discarded before binning the data to have $S/N \geq 5$ in each bin. To produce a background-subtracted X-ray light curve of IGR J17407−2808, we selected single- and double-pixel events from the EPIC-pn camera in the 0.2−10.0 keV energy band and used a time binning of 200 s.

3.3. ESO VLT

We observed the field of 2XMM J185114.3−000004 with the ESO VLT equipped with NAos COnica (NACO), the adaptive optics (AO) NIR imager and spectrometer mounted at the VLT UT4 telescope, in the J and Ks-bands. Observations were carried out on 2012 July 12 starting at 07:36:01.548 UT (see Table 4). We used the S27 camera, which has a pixel size of 0.027″ and a FOV of 28″ × 28″. The visual dichroic element and wavefront sensor were used. Image reduction was carried out using the

NACO pipeline data reduction, part of the ECLIPSE[4] package. Unfortunately, the observations were affected by natural seeing in excess of 1″, with a resulting poor resolution. Astrometry was carried out by using the 2MASS[5] catalogues as reference. Aperture photometry was performed with the PHOTOM task of the STARLINK package[6]. The photometric calibration was made against the 2MASS catalogue.

3.4. Other data

INTEGRAL data were only used for the source IGR J18175−2419 and the corresponding results are described in Sect. 4.3.

4. Results

4.1. 2XMM J185114.3−000004

The source 2XMM J185114.3−000004 triggered the BAT on 2012 June 17 at T_0 = 15:46:55 UT (64 s image trigger = 524542, Barthelmy et al. 2012), resulting in a 7σ detection. *Swift* performed an immediate slew to the target and XRT started observing at T_0+172 s. The AT (sequence 00524542000-001) ran for seven orbits until T_0 + 17.5 ks. Follow-up observations were obtained daily (sequences 00524542002−010). Additional target of opportunity (TOO) observations were first performed when the source rebrightened a few days later (PI P. Romano, sequences 00524542011−017), and then also on August 8−31 of the same year (PI P. Romano, sequences 00032512001−005). The *Swift* data therefore cover the first 18 days after the beginning of the outburst, and then about three weeks more, later that year (see Table 1). The source is only detected in five observations (00524542000−1 and 9, 00032512001 and 5). We also found an archival *Swift* serendipitous observation performed on 2012 November 20 (00044565001), which also resulted in a non-detection of the source.

We used 4 ks of the XRT/PC mode data collected during the outburst in 2012 June 17 and the simultaneous *Swift*/UVOT images to obtain an astrometrically corrected source position (see Evans et al. 2009; Goad et al. 2007) at: RA(J2000) = $18^h51^m14\overset{s}{.}50$, Dec(J2000) = −00°00′04″.1 (90% confidence level, c.l., uncertainty of 1″.7). This position is 1″.7 from the catalogued position of 2XMM J185114.3−000004. It is also 0″.6 from the Two Micron All Sky Survey source 2MASS J18511447−0000036 (Skrutskie et al. 2006).

Figure 1 shows the *Swift* BAT (14−50 keV) and XRT (0.2−10 keV) light curves of the source extracted from the first orbit of data collected at the beginning of the 2012 June outburst, while Fig. 2 shows the light curve derived from the whole XRT dataset. The XRT light curve reached a maximum of 4.1 counts s^{-1}. This corresponds to an approximate flux of 7.9×10^{-10} erg cm^{-2} s^{-1} (we used the conversion factor derived from the fit to the XRT data in observation 00524542000 PC mode, see Table 1). The lowest X-ray flux from the source was recorded at 3.8×10^{-3} counts s^{-1} during the observation 00524542001, thus resulting in an XRT dynamical range $\gtrsim 10^3$.

The BAT spectrum of the source extracted from observation 00524542000 was fit in the 14−70 keV energy range with a simple power law (see Table 1). The XRT spectrum extracted from observation 00524542000 was fit in the 0.3−10 keV energy range with an absorbed power law (see Table 1). We then considered the total BAT spectrum and the nearly simultaneous XRT spectrum for a broadband fit. Factors were included in the fitting to allow for the different exposures of the two spectra, normalisation uncertainties between the two instruments (generally constrained within ∼10%), and a likely spectral variation throughout the exposure.

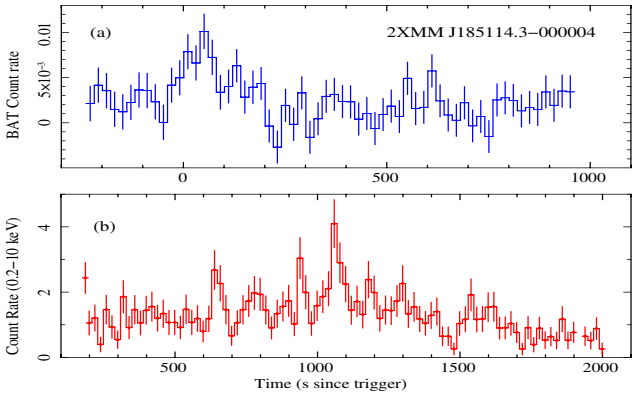

Fig. 1. Light curves of the outburst in 2012 June 17 of 2XMM J185114.3−000004 (first *Swift* orbit data). **a)** BAT light curve in the 14−50 keV with a time binning of 20 s. **b)** XRT light curve in the 0.2−10keV, rebinned to have at least 10 counts bin^{-1}. Note the different x-axis scales.

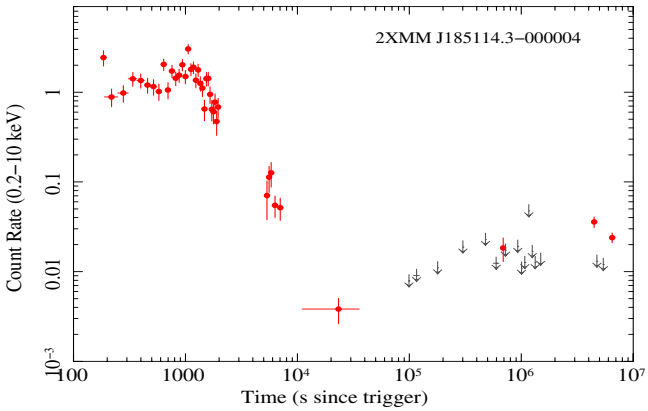

Fig. 2. *Swift*/BAT and XRT light curve obtained from the entire XRT dataset on 2XMM J185114.3−000004. Grey downward-pointing arrows correspond to the 3σ upper limits.

Several models typically used to describe the X-ray emission from accreting pulsars in HMXBs were adopted (e.g. White et al. 1983; Coburn et al. 2002; Walter et al. 2015, and references therein), including: (i) an absorbed power law (hereafter POW); (ii) an absorbed power law with high-energy exponential roll-off at an e-folding energy E_f (PHABS*CUTOFFPL in XSPEC, hereon CPL); (iii) and an absorbed power law with a high-energy cut-off at an energy E_c, and an e-folding energy E_f (PHABS*POWER*HIGHECUT, hereon HCT). The results for 2XMM J185114.3−000004 are reported in Table 5. The PL model clearly yielded unacceptable results. The CPL model produced significantly better results and gave $N_H = (13 \pm 4) \times 10^{22}$ cm^{-2}, $\Gamma = 0.11^{+0.68}_{-0.65}$, and $E_f = 10^{+7}_{-3}$ keV (see Fig. 3). These values are compatible with those usually expected for highly magnetised accreting NSs, SFXTs in particular (e.g. Romano et al. 2011c). The HCT model is, on the other hand, unable to constrain the cut-off energy (see Table 5); since the addition of one free parameter does not improve the statistics significantly

[4] http://www.eso.org/projects/aot/eclipse/
[5] http://www.ipac.caltech.edu/2mass/
[6] http://starlink.eao.hawaii.edu/starlink

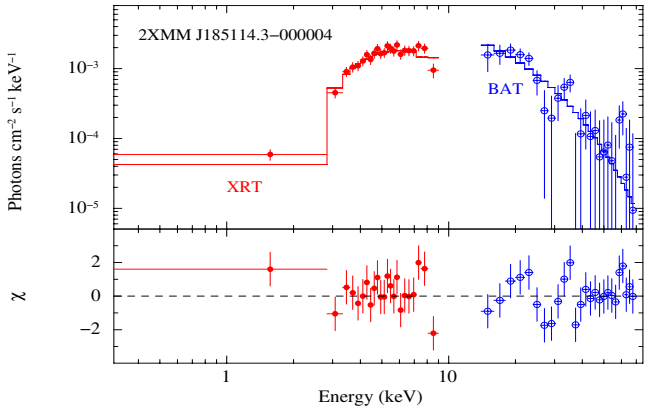

Fig. 3. Spectroscopy of the 2012 June 17 outburst of 2XMM J185114.3−000004. The *top panel* shows simultaneous XRT/PC (filled red circles) and BAT data (empty blue circles) fit with a PHABS*CUTOFFPL model. The residuals from the best fit are shown in the *bottom panel* (in units of standard deviations).

Table 5. Spectral fits of the simultaneous XRT and BAT data of 2XMM J185114.3−000004 during the outburst on 2012 June 17.

Model [a]	$N_{\rm H}$ (10^{22} cm^{-2})	Γ	$E_{\rm c}$ (keV)	$E_{\rm f}$ (keV)	$F^{b}_{0.5-100\,\rm keV}$ (erg cm^{-2} s^{-1})	χ^2/d.o.f.
POW	24^{+4}_{-3}	2.1 ± 0.4	–	–	3.8 ± 1.1	93.7/67
CPL	13 ± 4	$0.11^{+0.68}_{-0.65}$	–	10^{+7}_{-3}	1.7 ± 0.2	69.3/66
HCT	11 ± 4	$0.17^{+1.24}_{-0.42}$	5^{+16}_{-5}	10^{+5}_{-4}	1.7 ± 0.3	68.0/65

Notes. [(a)] POW = absorbed power law. CPL = power law with high-energy exponential with e-folding energy at $E_{\rm f}$ (keV). HCT = absorbed power law with a high-energy cut-off at $E_{\rm c}$ and e-folding energy $E_{\rm f}$. [(b)] Unabsorbed flux in units of 10^{-9} erg cm^{-2} s^{-1}.

(F-test probability of 0.269 with respect to the CPL model), we favour the CPL model.

The UVOT data obtained simultaneously with the XRT ones only yield 3σ upper limits in all filters (see Table 4). This is not surprising, given that the reddening along the line of sight (LOS) is $E(B-V) \sim 19$, implying an extinction of $A_V \sim 60$ mag.

By using our ESO VLT observations, inside the XRT error circle we detect a single source at the following position: RA(J2000) = 18$^{\rm h}$51$^{\rm m}$14$^{\rm s}$.48, Dec(J2000) = −00°00′03″.6 (90% c.l. associated uncertainty 0″.3). At the epoch of our observation, we measure for this source J = 15.8 ± 0.1 mag and Ks = 11.7 ± 0.1 mag (Vega system; not corrected for Galactic extinction, see Table 4). This source is present in the 2MASS catalogue (2MASS J18511447−0000036), with magnitudes $J > 15.6$ mag, H = 13.23 ± 0.07 mag, and K = 11.80 ± 0.04 mag, in agreement with our measurements.

2XMM J185114.3−000004 was detected by the EPIC-pn at an average count-rate (0.5−10 keV) of (9.4 ± 0.7) × 10^{-3} count s^{-1} in obs. 0017740401 and (3.5 ± 0.5) × 10^{-3} count s^{-1} in obs. 0017740501. The corresponding EPIC-pn spectrum could be well fit in both cases, with an absorbed power-law model (see Table 1).

Given the relatively low count-rate of the source, we combined in each of the two observations the EPIC-pn and MOS spectra by following the online SAS data analysis threads[7]. The resulting spectra (shown in Fig. 5) provided values for the best-fit parameters in agreement with those estimated above by using only the EPIC-pn data (to within the uncertainties).

In obs. 0017740401, where the statistics was better, we also inspected the source light curve and event file, searching for timing features. However, the statistics was far too poor to provide a meaningful timing analysis.

The source was not detected in obs. 0671510101. From the EPIC-pn data we estimated a 3σ upper limit on the source count-rate of 8 × 10^{-4} in the 0.5−10 keV energy range. Assuming the same spectral shape as in obs. 0017740501, the count-rate upper limit would translate into a flux of $F_{0.5-10\,\rm keV} < 4 \times 10^{-15}$ erg cm^2 s^{-1}.

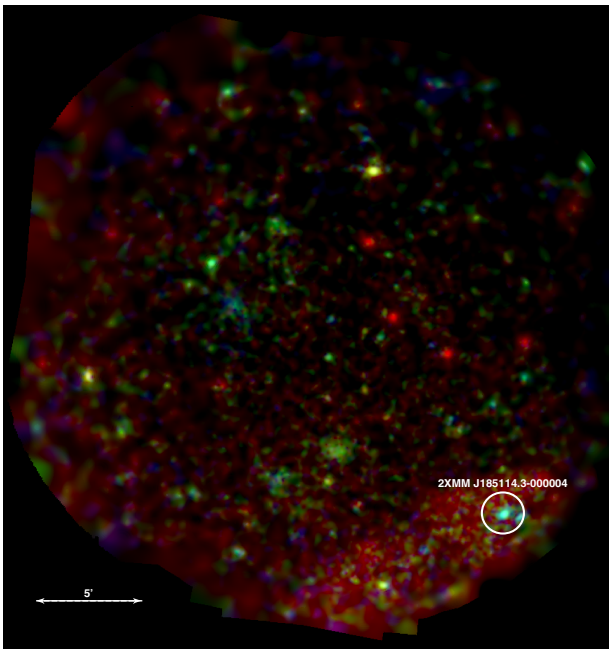

Fig. 4. *XMM-Newton* FOV of the observations 0017740401 and 0017740501, detector background subtracted, vignetting corrected, combining EPIC-pn and MOS. Red, green, and blue correspond to 0.5−2.0 keV, 2.0−4.5 keV, and 4.5−12 keV. The diffuse emission around 2XMM J185114.3−000004 is due to SNR G32.8−0.1.

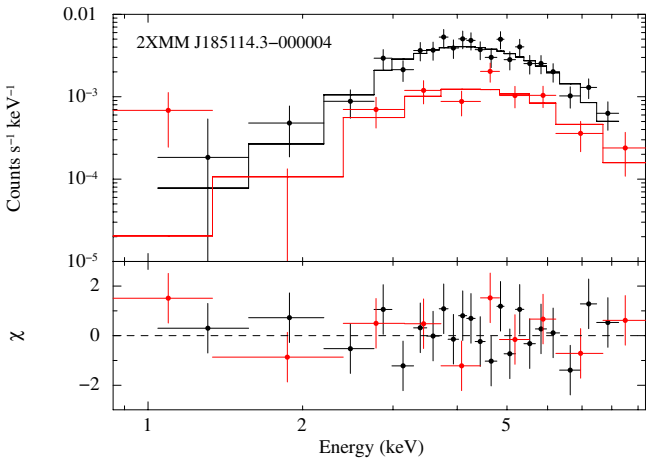

Fig. 5. Merged *XMM-Newton* EPIC-pn+MOS1+MOS2 spectra extracted from the observations 0017740401 (black) and 0017740501 (red). The best-fit model is obtained with an absorbed power law. The residuals from the fit are shown in the *bottom panel*.

[7] See http://xmm.esac.esa.int/sas/current/documentation/threads/epic_merging.shtml

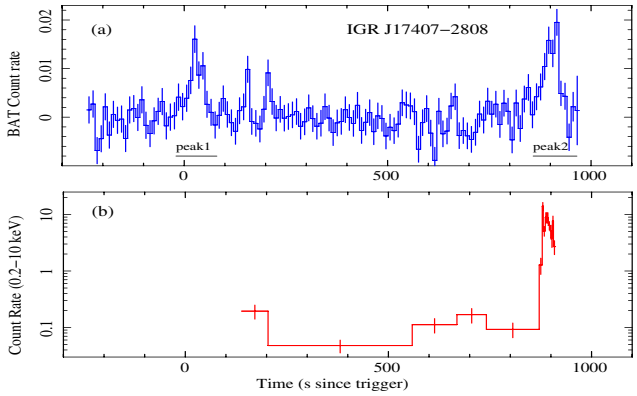

Fig. 6. Light curves of the 2011 October 15 outburst of IGR J17407−2808 (first *Swift* orbit data). **a)** BAT light curve in the 14−50 keV energy band and a binning of 10 s. The horizontal lines mark the time intervals used for the spectral extraction (peak1 and peak2). **b)** The XRT light curve in the 0.2−10 keV energy band. An adaptive binning has been used to achieve in each point a signal-to-noise ratio of $S/N = 3$.

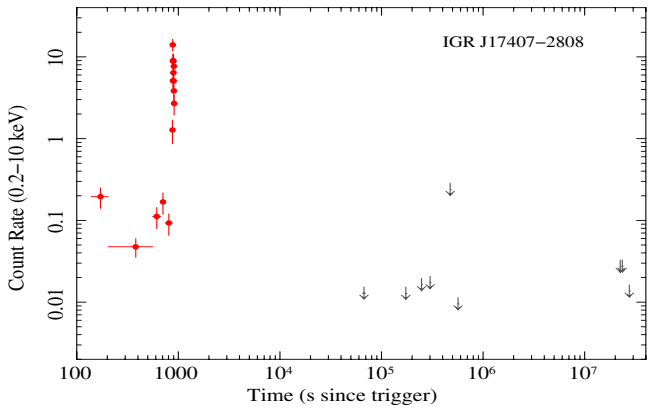

Fig. 7. Light curve of the XRT dataset of IGR J17407−2808. Grey downward-pointing arrows correspond to the 3σ upper limits calculated for the source non-detections. Points after 10^7 s correspond to serendipitous observations.

4.2. IGR J17407−2808

The source IGR J17407−2808 triggered the BAT on 2011 October 15 at T_0 = 01:12:40 UT (image trigger = 505516, Romano et al. 2011a). *Swift* immediately slewed to the target and XRT started observing at T_0+131 s. The AT (sequence 00505516000) ran for two orbits until T_0 + 6.6 ks. However, owing to a loss of lock of the star tracker, only the first orbit has a stable attitude and can be used for scientific analysis. Follow-up pointings toward the source were obtained daily as TOO observations (PI P. Romano, sequences 00036122001−007, see Table 2). The source was only detected during the AT observation (00505516000), but never in the following monitoring campaigns and in the serendipitous observations found in the *Swift* archive (see Table 2).

We used 772 s of XRT/PC mode data and the simultaneously collected UVOT images to obtain the best astrometrically-corrected source position at: RA(J2000) = $17^h40^m42\overset{s}{.}10$, Dec(J2000) = $-28°07'26\overset{''}{.}0$. The associated uncertainty at 90% c.l. is $2\overset{''}{.}4$. This position is $1\overset{''}{.}5$ from CXOU J174042.0−280724, so we can confirm the association between the two sources, as preliminarily reported by Romano et al. (2011a).

Figure 6 shows the BAT (14−50 keV) and XRT (0.2−10 keV) light curves of the first orbit of data while, in Fig. 7, we plot the light curve derived from the whole XRT dataset. Around T_0 + 900 s, the source displayed a sharp rise in count-rate increasing the level of its soft X-ray emission by a factor of 125 in ∼266 s. A peak count-rate of about 14 counts s^{-1} is recorded in the light curve binned at $S/N = 3$. This corresponds to a flux of $\sim 2.3 \times 10^{-9}$ erg cm^{-2} s^{-1} when using the conversion factor derived from the fit to the XRT data in observation 00505516000 (see Table 2). Since the lowest point (obtained from observation 00036122007) was a 3σ upper limit at 9.5×10^{-3} counts s^{-1}, the overall dynamical range revealed by XRT is in excess of ∼1400.

We extracted two distinct BAT spectra that cover the two peaks in the BAT light curve (see Fig. 6a), i.e. from T_0 − 20 to 80 s (peak1) and from T_0 + 858 to 965 s (peak2). We fit them with a power law and the results are reported in Table 2).

The XRT spectrum extracted from obs. 00505516000 was fit in the 0.3−10 keV energy range using Cash (1979) statistics with an absorbed power law. We measured an absorption column density $N_H = (0.84^{+2.00}_{-0.84}) \times 10^{22}$ cm^{-2} consistent with the expected Galactic value in the direction of the source ($N_H^{Gal} = 0.727 \times 10^{22}$ cm^{-2}, Kalberla et al. 2005), and a power-law photon index $\Gamma = -0.45^{+0.86}_{-0.71}$, as reported in Table 2.

Since no spectral variations could be detected in either the BAT data or in the XRT data owing to the low signal, we fit together the BAT peak2 spectrum and the XRT spectrum extracted by using all exposure time available. Factors were included in the fitting to allow for normalisation uncertainties between the two instruments, the different exposures of the two spectra, and a likely spectral variation throughout the exposure.

The spectra were fit with the models that typically describe either HMXBs (see Sect. 4.1), or low mass X-ray binaries (LMXB, Done et al. 2007; Paizis et al. 2006; Del Santo et al. 2010; Wijnands et al. 2015). The results are presented in Table 6. The POW fit was not acceptable because of large residuals. The CPL fit yields $\Gamma = -0.76^{+0.49}_{-0.53}$ and $E_f = 13^{+5}_{-3}$ keV (see Fig. 8). In this fit, we fixed the absorption column density to the value determined from the XRT data alone, i.e. $N_H = 0.84 \times 10^{22}$ cm^{-2}. The HCT model cannot properly constrain the cut-off energy; since the addition of one free parameter does not significantly improve the fit (F-test probability of 0.423), we favour the CPL model. A fit with an absorbed black body (with N_H fixed at 0.84×10^{22} cm^{-2}) also yielded acceptable results. In this case, the estimated black-body temperature of about 8 keV would be roughly consistent with that reported previously by Sguera et al. (2006). A fit with an absorbed bremsstrahlung model yields a very high temperature and suffers from large systematics in the residuals, so we consider it unacceptable. Fits with more sophisticated models, such as a Comptonisation model (PHABS*(COMPTT)) and an accretion disk model with multiple black-body components (PHABS*(DISKBB+POWER)) could not significantly improve the fits. Furthermore, the majority of the spectral fit parameters of these models turned out to be largely unconstrained owing to the limited statistics of the data.

The source was not detected in any UVOT data obtained simultaneously with XRT. The corresponding 3σ upper limits in all filters were of u = 20.23, b = 18.61, v = 17.56, $m2$ = 20.90, $w1$ = 20.64, and $w2$ = 20.33 mag (Vega system, not corrected for Galactic extinction).

IGR J17407−2808 was also observed serendipitously during an *XMM-Newton* observation performed on 2016 March 6. The 0.2−10.0 keV energy band light curve, at a binning of 200 s, reported in Fig. 9 shows three moderately bright flares, reaching between 0.1 and 0.3 counts s^{-1}. The *XMM-Newton* spectra of

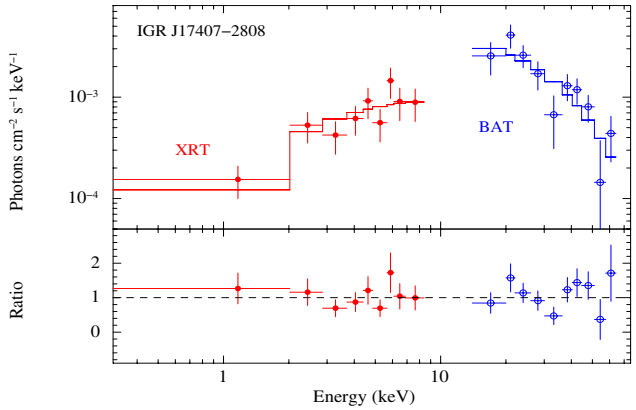

Fig. 8. Spectroscopy of the 2011 October 15 outburst of IGR J17407−2808. *Top panel*: simultaneous XRT/PC data (filled red circles) and BAT data (empty blue circles) fit with a PHABS*CUTOFFPL model. *Bottom panel*: the ratio between the data and the best-fit model.

Table 6. Spectral fits of the simultaneous XRT and BAT data of IGR J17407−2808 during the outburst on 2011 October 15.

Model[a]	$N_{\rm H}$ (10^{22} cm^{-2})	Γ	$E_{\rm c}$ (keV)	$E_{\rm f}$ (keV)	$F^{b}_{0.5-100\,\rm keV}$ (erg cm^{-2} s^{-1})	χ^2/d.o.f.
POW	$5.3^{+2.2}_{-1.7}$	$1.6^{+0.4}_{-0.4}$	–	–	6.5 ± 1.1	124/93
CPL	0.84^{c}	$-0.76^{+0.49}_{-0.53}$	–	13^{+5}_{-3}	3.9 ± 0.7	85.3/93
HCT	$0.84^{+1.87}_{-0.84}$	$-0.45^{+0.72}_{-0.68}$	20^{+6}_{-20}	14^{+8}_{-4}	3.6 ± 0.7	83.7/91
		kT (keV)				
BB	0.84^{c}	$8.7^{+0.6}_{-0.5}$	–	–	3.6 ± 0.6	83.4/94
BRE	$4.5^{+1.8}_{-1.4}$	65^{+113}_{-28}	–	–	6.0 ± 0.9	114.9/93

Notes. [(a)] POW = absorbed power law. CPL = power law with high energy exponential with e-folding energy at $E_{\rm f}$ (keV). HCT = absorbed power law with a high energy cut-off at $E_{\rm c}$ and e-folding energy $E_{\rm f}$. BB = black body with temperature kT. BRE = thermal bremsstrahlung with plasma temperature kT. [(b)] Unabsorbed flux in units of 10^{-9} erg cm^{-2} s^{-1}. [(c)] Fixed to the value obtained from the fit to the XRT data (see Table 2).

the source could be well described by using an absorbed power-law model (Fig. 10), and an $N_{\rm H} = (0.77^{+0.70}_{-0.48}) \times 10^{22}$ cm^{-2}, consistent with the Galactic value, and with the results obtained with the XRT data. The absorbed 0.5−10 keV flux is 5.4×10^{-13} erg cm^{-2} s^{-1}, the lowest X-ray flux measured for this source, enhancing its previously estimated dynamic range (with XRT) up to >4000.

4.3. IGR J18175−2419

IGR J18175−2419 was observed by *Swift* as part of our ongoing effort (Romano 2015) to study SFXTs, candidate SFXTs, and classical supergiant HMXBs through long-term monitoring programs with the XRT (see Romano et al. 2014a, for recent results). Our monitoring campaign (see Table 3) was performed from 2016 March 6 to 14 for 1 ks a day. As the source was poorly known, the XRT was set in AUTO mode to best exploit the automatic mode-switching of the instrument in response to changes in the observed fluxes (Hill et al. 2004). We collected a total of 9 *Swift* observations for a total net XRT exposure time of ∼7 ks. No source was detected within the previously reported INTEGRAL error circle (Grebenev 2013) in either any of the 1 ks snapshots or in the combined total

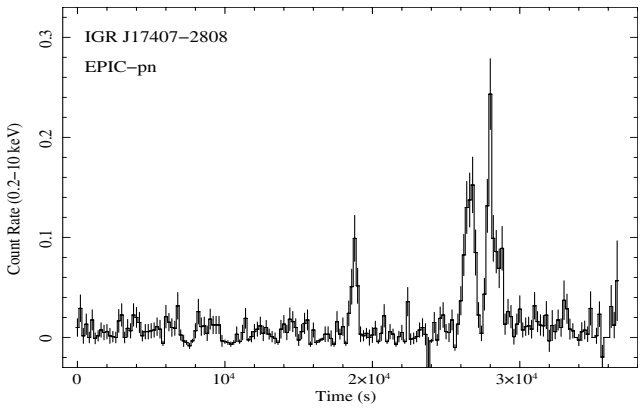

Fig. 9. *XMM-Newton* EPIC-pn light curve of IGR J17407−2808 extracted from the observation 0764191301, with a 200 s binning.

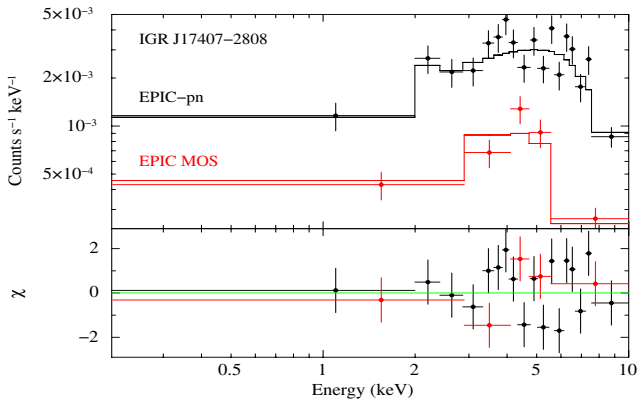

Fig. 10. *XMM-Newton* EPIC-pn (black) and MOS1 (red) spectra extracted from observation 0764191301. The best fit is obtained by using an absorbed power-law model. The residuals from the fits are shown in the *bottom panel*.

exposure. We estimated a 3σ upper limit on the source X-ray count rate of $1.5–3 \times 10^{-3}$ counts s^{-1}, which corresponds to $0.8–1.7 \times 10^{-13}$ erg cm^{-2} s^{-1} (when using, within PIMMS, a typical spectral model for SFXTs, comprising a power law with photon index $\Gamma = 1.5$ and an absorption column density corresponding to the Galactic value in the direction of the source, i.e. $N_{\rm H}^{\rm Gal} = 2.66 \times 10^{21}$ cm^{-2}).

As no significant emission was detected with *Swift*/XRT at the best known position of IGR J18175−2419 down to a luminosity that is usually fainter than that of SFXTs in quiescence, we reanalysed the INTEGRAL data in which the source was discovered. INTEGRAL observations are divided into so-called science windows (SCWs), i.e. pointings with typical durations of ∼2−3 ks. The only source detection is reported in Grebenev (2013), where the IBIS/ISGRI data collected in the direction of the X-ray nova SWIFT J174510.8−2624 on 2012 September 26 at 14:57 (UT) were analysed using the software developed at the Space Research Institute of the Russian Academy of Sciences (Revnivtsev et al. 2004; Krivonos et al. 2010). The detection of the source with the highest significance was obtained during the SCW 51 in the satellite revolution 1215. The source was also reported to be visible during the first 10 min of the SCW 52 in the same revolution, albeit with a lower significance. We analysed these two SCWs by using version 10.2 of the Off-line Scientific Analysis software (OSA) distributed by the ISDC (Courvoisier et al. 2003).

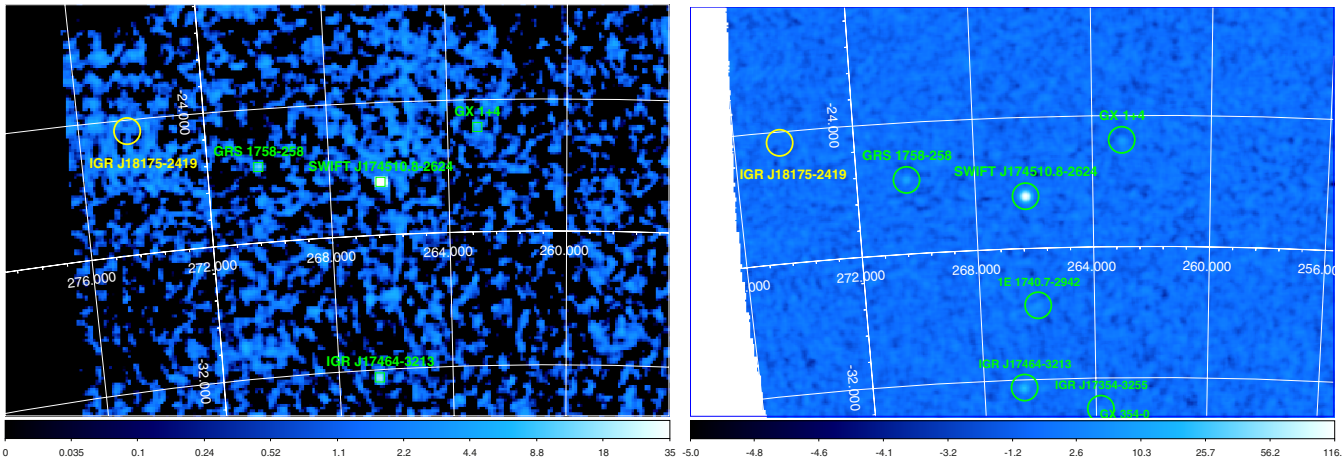

Fig. 11. *Left*: IBIS/ISGRI mosaic extracted with the OSA software from the SCW 51 in revolution 1215 (20−80 keV energy band). We indicated (green squares) on the mosaic the position of 4 sources detected with a sufficiently high significance (SWIFT J174510.8−2624, GRS 1758−258, GX 1+4, IGR J17464−3213) and that previously reported for IGR J18175−2419. The latter is indicated by using a yellow circle with a radius of 24′ centred on the source best position provided by Grebenev (2013). *Right*: significance map obtained with the BATIMAGER software (Segreto et al. 2010a) in the 20−80 keV energy band for the SCW 51. Green circles (24′ radius) shows the positions of all sources significantly detected in the field, as well as the position of IGR J18175−2419, as reported by Grebenev (2013). In either mosaic, independently built with different software, we do not detect any significant emission from IGR J18175−2419. The bars at the bottom of each mosaic indicate the colour codes for the detection significances in units of standard deviations.

Following Grebenev (2013), we first extracted the IBIS/ISGRI mosaic of the SCW 51 in the 20−80 keV energy band and searched for the source previously reported at the best determined position of RA(J2000) = $18^h17^m52\overset{s}{.}8$, Dec(J2000) = $-24°19'45\overset{''}{.}0$ (the associated uncertainty is 4′). The mosaic is shown in Fig. 11 (left). We did not detect any significant emission around the position of the source, which lies at an off-axis angle of about 14 deg from the center of the instrument FOV. At these large off-axis positions, the calibration of the instrument becomes gradually more uncertain and it is difficult to estimate a reliable upper-limit on the X-ray flux. By using the MOSAIC_SPEC tool, the derived 3σ upper limit on any source count-rate at this position is of 8.4 counts s^{-1} in the 20−80 keV energy band (effective exposure time 3281 s), corresponding to roughly 40 mCrab[8] (i.e., 6×10^{-10} erg cm^{-2} s^{-1}). This is a factor of 2.5 lower than the flux of the source reported by Grebenev (2013).

For completeness, we also extracted the IBIS/ISGRI mosaic of the combined SCW 50, 51, and 52. This matches the time interval of the light curve shown in Fig. 2 of Grebenev (2013). Also in this case, no significant emission from the position of IGR J18175−2419 is detected. The estimated 3σ upper limit is 15 mCrab (i.e., 2×10^{-10} erg cm^{-2} s^{-1}) in the 20−80 keV energy band (effective exposure time 9890 s).

To further check the source detection, we used an independently developed software, the BATIMAGER, designed to generate sky maps for generic coded mask detectors and optimised, in particular, for the processing of *Swift*/BAT and INTEGRAL/ISGRI data. Detailed description and performance of the software when applied on the BAT survey data is given in Segreto et al. (2010a), while its imaging performance, when applied to the IBIS/ISGRI data, are reported in Segreto et al. (2008, 2010b). Figure 11 (right) shows the significance map of the region around IGR J18175−2419 obtained with the BATIMAGER software in the 20−80 keV energy band by using the data in SCW 51. The significantly detected sources in the image are indicated with green circles, confirming that no source is present at the previously reported position of IGR J18175−2419 (Grebenev 2013).

Given the above results, we suggest that the source IGR J18175−2419 was erroneously reported. This might have occurred owing to some mosaic reconstruction problem at the large off-axis angle where IGR J18175−2419 should have been located. We thus do not discuss this source any further in this paper.

5. Discussion and conclusions

5.1. 2XMM J185114.3−000004

The BAT image trigger on the transient 2XMM J185114.3−000004 was a long (64 s) and strong (7σ) one. The XRT arcsecond position we provide for this source (refinement of Barthelmy et al. 2012), with an uncertainty of $1\overset{''}{.}7$ at 90% c.l., is consistent with the catalogued position of 2XMM J185114.3−000004 and is only $0\overset{''}{.}6$ from 2MASS J18511447−0000036 ($J > 15.6$, $H = 13.23 \pm 0.07$, $K = 11.80 \pm 0.04$). This IR source, which we observed with NACO at VLT obtaining $J = 15.8 \pm 0.1$ mag and $Ks = 11.7 \pm 0.1$ mag, can therefore be safely considered the IR counterpart of 2XMM J185114.3−000004 (finally removing the need for the cautionary statements on this association raised by Bamba et al. 2016). Even though optical spectroscopic data for this source are not yet available, and the presence of a supergiant companion cannot be firmly established, we show below that all measured properties favour the association of 2XMM J185114.3−000004 with the SFXT class.

The BAT light curve of the source (Fig. 1) starts with a bright flare, lasting about 100 s (FWHM, when fit with a Gaussian), that reached about $\sim 10^{-9}$ erg cm^{-2} s^{-1} (15−50 keV). The overall duration of the outburst is much longer than this (Fig. 2), since XRT caught several flares in the monitoring observations following the main event. The brightest of these flares occurred at $T \sim T_0 + 1050$ s and reached $\sim 8 \times 10^{-10}$ erg cm^{-2} s^{-1} (0.2−10 keV).

[8] The conversion from count-rate to mCrab was carried out by using the most recent observations of the Crab (at the time of writing) in spacecraft revolution 1597. From these data, we measured for the Crab a count-rate of 214.6 ± 0.3 counts s^{-1} from the IBIS/ISGRI mosaics in the 20−80 keV energy band.

After the first slew, the XRT data show a steep decay lasting until $T + 23$ ks, which is typical of the SFXT population (see Fig. 4, in Romano 2015), with a behaviour strongly reminiscent of, for example, the 2005 August 30 flare of IGR J16479−4514. The dynamical range of the initial flare is about three orders of magnitude, but the overall soft X-ray dynamical range reaches ≳4000 when including the archival *XMM-Newton* data. We note that, when using a distance of 12 kpc (see below), the observed luminosities range between $L \sim 5 \times 10^{33}$ and 2.6×10^{37} erg s^{-1}. This is the typical range of an SFXT source.

The broadband spectrum of 2XMM J185114.3−000004 (Fig. 3), presented here for the first time, can be well described by an absorbed cut-off power law model, with $\Gamma = 0.11^{+0.68}_{-0.65}$ and $E_{\rm f} = 10^{+7}_{-3}$ keV, values which are well within the distribution of parameters measured for HMXB hosting relatively young NSs (see Romano 2015). The measured absorption ($N_{\rm H} = (13 \pm 4) \times 10^{22}$ cm^{-2}) is much larger than the expected Galactic value in the direction of the source ($N_{\rm H}^{\rm Gal} = 1.54 \times 10^{22}$ cm^{-2}, Kalberla et al. 2005), as expected in SFXTs owing to the presence of a dense stellar wind. We note (see Fig 4) that there is diffuse emission along the LOS to 2XMM J185114.3−000004 that may contribute to the reddening. This emission is uncorrelated to 2XMM J185114.3−000004 and due to the nearby supernova remnant SNR G32.8−0.1 as discussed in Bamba et al. (2016).

Assuming therefore a blue supergiant nature for the donor star of the 2XMM J185114.3−000004 system, we can determine the reddening toward the source by considering its intrinsic NIR color as per Wegner (1994). In the present case, we obtain $J-K = 4.1$, whereas the intrinsic value of this colour is $(J-K)_0 \sim 0$ for early-type supergiants, which implies a color excess of $E(J-K) \sim 4.1$. Using the Milky Way extinction law of Cardelli et al. (1989), this implies a reddening $A_V \approx 20$ mag, or $A_K \approx 2$ mag. This absorption amount is consistent with the non-detection of the object at ultraviolet and optical bands, as found from the UVOT data analysis.

This quantity of reddening, when using the formula of Predehl & Schmitt (1995), implies a column density $N_{\rm H} \sim 3.6 \times 10^{22}$ cm^{-2}, which is lower than both that of the Galaxy along the LOS of the source (see Sect. 4.1), and that measured in X-rays. This indicates that (i) the object lies within the Galaxy and (ii) additional X-ray extinction is present around the accretor, likely produced by the accreting material as observed in many other HMXBs and SFXTs.

As regards point (i), we can try to estimate the distance of the system under the assumption that it hosts an OB supergiant. Using $A_V \sim 20$ mag and the tabulated absolute magnitudes (Lang 1992) and colours (Wegner 1994) for this type of stars, we find a distance of ∼12 kpc. This would place the source on the Galactic plane beyond the Sagittarius-Carina arm tangent and close to (or possibly within) the Perseus arm, according to the Galaxy map of Leitch & Vasisht (1998).

5.2. IGR J17407−2808

The nature of the hard X-ray transient IGR J17407−2808 has been quite controversial since its discovery. Sguera et al. (2006) reported three short bright flares reaching 10^{-8} erg cm^{-2} s^{-1} in the 20−60 keV band and proposed the association of this object with the SFXT class. These authors could not exclude different possibilities, as that of a new "burst-only" source (Cocchi et al. 2001; Cornelisse et al. 2002). The search for a soft X-ray counterpart for IGR J17407−2808 led Heinke et al. (2009) to propose CXOU J174042.0−280724 as a likely candidate because of the observed flaring variability common to both systems. Their *Chandra* observations revealed CXOU J174042.0−280724 as a fast transient source, varying around a level of 10^{-13}−10^{-12} erg cm^{-2} s^{-1} and thus suggesting the presence of an accreting black hole or neutron star. Heinke et al. (2009) ruled out the presence of a supergiant companion for any distance larger than 10 kpc, and showed that an LMXB or a Be X-ray binary beyond 10 kpc were more likely possibilities. Based on our preliminary position (Romano et al. 2011a), Greiss et al. (2011) found a candidate NIR counterpart 0.″67 from the *Chandra* position in archival VVV survey data. They find moderate reddening along its LOS and de-reddened optical and NIR magnitudes and colours consistent with a late type-F dwarf (at a distance of ∼3.8 kpc). This would thus also disfavour the SFXT hypothesis, unless the F star is a foreground object. Kaur et al. (2011) confirmed the values of the previously reported optical magnitudes and found that the candidate counterpart was about one magnitude brighter four days after the detected flares observed by *Swift*. This is something expected in outbursting LMXBs owing to the irradiation of the optical star by the X-rays emitted from the compact object.

Thanks to the fact that IGR J17407−2808 triggered the BAT, we obtained simultaneous soft X-ray coverage of the source while it was rapidly decaying, and we can now unequivocally establish that the soft X-ray counterpart of IGR J17407−2808 is indeed CXOU J174042.0−280724 (see our preliminary results in Romano et al. 2011a). The *Swift*/BAT light curve (Fig. 6a) shows at least two bright flares reaching a few 10^{-9} erg cm^{-2} s^{-1} (15−50 keV), whose profiles are symmetrical and narrow, lasting about 15−20 s (FWHM, when fitted with a Gaussian shape). These values are about a factor of 10 shorter than has been measured for typical SFXTs and for 2XMM J185114.3−000004. The second peak (peak2) is also clearly correlated with a soft X-ray flare (Fig. 6b) that reached $\sim 2 \times 10^{-9}$ erg cm^{-2} s^{-1} (0.5−10 keV) and that lasted at least 10 s, as the flare is truncated as a result of the satellite slew, so only a lower limit on its duration is available. When the source was once again within the XRT FOV, it was already below detection (Fig. 7), and all subsequent XRT observations of ≲1 ks exposures, never revealed the source again, yielding individual 3σ upper limits at the level of 10^{-12} erg cm^{-2} s^{-1} and a combined 3σ upper limit of 1.1×10^{-12} erg cm^{-2} s^{-1}. The serendipitous *XMM-Newton* observations that we analysed show, consistent with what has been seen in the *Chandra* data (Heinke et al. 2009), a relatively steady flux of a few 10^{-13} erg cm^{-2} s^{-1} with three equally symmetrical and narrow flares reaching 10^{-12} erg cm^{-2} s^{-1} (0.5−10 keV) and lasting between 190 and 385 s (FWHM). We note that such flares would go undetected in XRT observations of ∼1 ks. All the results thus confirmed that this is most likely the truly quiescent behaviour of IGR J17407−2808.

The source is therefore characterised by a relatively low, steady flux and infrequent episodes of more pronounced activity, with several short bright flares closely spaced in time ($\sim 10^3$ s). These flares often reach an X-ray flux that is only a few times higher than the persistent level but more rarely can achieve an X-ray dynamic range as high as 4 orders of magnitude. As the distance is unknown, the range of observed fluxes would correspond to luminosities of $L \sim 10^{33}$−10^{37} erg s^{-1} at 3.8 kpc (see before), or $L \sim 10^{34}$−10^{38} erg s^{-1} at 13 kpc.

The *Swift* AT data also provide the first simultaneous broadband spectroscopy for this transient. We obtained satisfactory fits with either an absorbed power law with a high energy rollover or an absorbed black body. The first model provided results that are reminiscent of those measured from SFXTs (see, e.g.

Romano et al. 2013; Romano 2015, for a review of the *Swift* spectra). The negative photon index remains, however, puzzling. The black-body model provides a quite unlikely high value of the temperature for an accreting object hosted in either an HMXB or LMXB. In both fits with the power law with a high-energy rollover and the black body, the absorption needed to be fixed to that obtained from the fit to the XRT data alone and was consistent with being as low as $N_{\rm H} = (0.84^{+2.00}_{-0.84}) \times 10^{22}$ cm^{-2}. This is comparable with the expected Galactic extinction in the direction of the source ($N_{\rm H}^{\rm Gal} = 0.727 \times 10^{22}$ cm^{-2}, Kalberla et al. 2005). In principle, this is much lower than the absorption column density expected for an HMXB or an SFXT, thus favouring the LMXB hypothesis. However, we also note that the SFXT IGR J08408−4503 usually displays an absorption column density $\ll 10^{22}$ cm^{-2} (Bozzo et al. 2010; Sidoli et al. 2010). On the other hand, the $N_{\rm H}$ obtained from the XRT data only, as well as from the fit with an absorbed power law with a high energy cutoff could still be consistent with the absorption column density expected for an HMXB or an SFXT.

The information collected so far on IGR J17407−2808 is therefore difficult to interpret. In the framework of the HMXB/SFXT nature of IGR J17407−2808, pro factors are the light curve flaring, which is characterized by at leat two orders of magnitude during the flare and the overall dynamic range of about four orders of magnitude. The spectral properties are also reminiscent of what is usually observed from these systems, even though the broadband properties of these systems are not always a distinctive feature (Romano et al. 2014a). Against the HMXB/SFXT hypothesis is the low LOS absorption, making it unlikely to hide a supergiant behind the F star, even when the F star is only a foreground source. The X-ray flares displayed by IGR J17407−2808 are also quite short compared to those of the SFXTs, which typically last a few thousands of seconds. The broadband spectral properties and the optical counterpart could be roughly consistent with those of a LMXB but the short flares displayed by IGR J17407−2808 and the fast variability are not commonly observed in LMXBs. The latter typically undergo weeks- to months-long outbursts regulated by the accretion disk instability (Lasota 2001) and might show additional flaring activity on top of this (see, for example, McClintock & Remillard 2006, for a review). The variability recorded by *Swift* and shown in Figs. 6 and 7 is thus not closely reminiscent of that displayed by either black holes or NS LMXBs in outburst. We note that the profiles and durations of the short flares emitted from IGR J17407−2808 do not resemble those of type-I X-ray bursts, thus also excluding the association between this object and the so-called burst only sources (Cornelisse et al. 2004). Given the relatively high luminosities recorded by *Swift* ($L \sim 10^{33}$−10^{37} erg s^{-1}) for any reasonable estimate of the source distance $\gtrsim$3.8 kpc, we consider it an even less likely possibility that IGR J17407−2808 is a white-dwarf binary (Sazonov et al. 2006). Similarly unlikely is the possibility that IGR J17407−2808 is a a very faint X-ray transient (VFXT, King & Wijnands 2006; Wijnands et al. 2006), since these objects show a photon index of about 1.5−2.2 in this luminosity range (see Degenaar & Wijnands 2010; Del Santo et al. 2007) and similar behaviour, even when showing hybrid outbursts (faint and bright; see Del Santo et al. 2010).

We conclude that IGR J17407−2808 is most likely an LMXB hosting an accreting compact object. However, the detailed nature of this source remains concealed and spectroscopic follow-up of the candidate optical counterpart are encouraged to achieve a more precise classification.

Acknowledgements. We thank the *Swift* team duty scientists and science planners for their courteous efficiency, and M. Capalbi, M. de Pasquale, P. A. Evans for helpful discussions. We also thank the referee for comments that helped improve the paper. P.R., B.S., and S.C. acknowledge contract ASI-INAF I/004/11/0. P.E. acknowledges funding in the framework of the NWO Vidi award A.2320.0076 (PI: N. Rea). L.D. acknowledges support by the Bundesministerium für Wirtschaft und Technologie and the Deutsches Zentrum für Luft und Raumfahrt through the grant FKZ 50 OG 1602. Based on observations made with ESO Telescopes at the Paranal Observatory under programme ID 089.D-0245(A). *XMM-Newton* is an ESA science mission with instruments and contributions directly funded by ESA Member States and NASA. The *XMM-Newton* project is supported by the Bundesministerium für Wirtschaft und Technologie/Deutsches Zentrum für Luft- und Raumfahrt (BMWI/DLR, FKZ 50 OR 1408) and the Max-Planck Society.

References

Bamba, A., Terada, Y., Hewitt, J., et al. 2016, ApJ, 818, 63
Barthelmy, S. D., Barbier, L. M., Cummings, J. R., et al. 2005, Space Sci. Rev., 120, 143
Barthelmy, S. D., Baumgartner, W. H., Burrows, D. N., et al. 2012, GRB Coordinates Network, 13367, 1
Bozzo, E., Falanga, M., & Stella, L. 2008, ApJ, 683, 1031
Bozzo, E., Stella, L., Ferrigno, C., et al. 2010, A&A, 519, A6
Bozzo, E., Romano, P., Ferrigno, C., Esposito, P., & Mangano, V. 2013, Adv. Space Res., 51, 1593
Bozzo, E., Romano, P., Ducci, L., Bernardini, F., & Falanga, M. 2015, Adv. Space Res., 55, 1255
Bozzo, E., Oskinova, L., Feldmeier, A., & Falanga, M. 2016, A&A, 589, A102
Burrows, D. N., Hill, J. E., Nousek, J. A., et al. 2005, Space Sci. Rev., 120, 165
Cardelli, J. A., Clayton, G. C., & Mathis, J. S. 1989, ApJ, 345, 245
Cash, W. 1979, ApJ, 228, 939
Coburn, W., Heindl, W. A., Rothschild, R. E., et al. 2002, ApJ, 580, 394
Cocchi, M., Bazzano, A., Natalucci, L., et al. 2001, A&A, 378, L37
Cornelisse, R., Verbunt, F., in't Zand, J. J. M., et al. 2002, A&A, 392, 885
Cornelisse, R., in't Zand, J. J. M., Kuulkers, E., et al. 2004, Nuc. Phys. B Proc. Suppl., 132, 518
Courvoisier, T., Walter, R., Beckmann, V., et al. 2003, A&A, 411, L53
Dalton, W. W., & Sarazin, C. L. 1995, ApJ, 440, 280
Degenaar, N., & Wijnands, R. 2010, A&A, 524, A69
Del Santo, M., Sidoli, L., Mereghetti, S., et al. 2007, A&A, 468, L17
Del Santo, M., Sidoli, L., Romano, P., et al. 2010, MNRAS, 403, L89
Done, C., Gierliński, M., & Kubota, A. 2007, A&ARv, 15, 1
Ducci, L., Doroshenko, V., Romano, P., Santangelo, A., & Sasaki, M. 2014, A&A, 568, A76
Evans, P. A., Beardmore, A. P., Page, K. L., et al. 2009, MNRAS, 397, 1177
Farinelli, R., Romano, P., Mangano, V., et al. 2012, MNRAS, 424, 2854
Gehrels, N., Chincarini, G., Giommi, P., et al. 2004, ApJ, 611, 1005
Goad, M. R., Tyler, L. G., Beardmore, A. P., et al. 2007, A&A, 476, 1401
Götz, D., Mereghetti, S., Mowlavi, N., & Soldan, J. 2004, GCN Circ., 2793, 1
Grebenev, S. A. 2013, Astron. Lett., 39, 661
Grebenev, S. A., & Sunyaev, R. A. 2007, Astron. Lett., 33, 149
Greiss, S., Steeghs, D., Maccarone, T., et al. 2011, ATel, 3688
Heinke, C. O., Tomsick, J. A., Yusef-Zadeh, F., & Grindlay, J. E. 2009, ApJ, 701, 1627
Hill, J. E., Burrows, D. N., Nousek, J. A., et al. 2004, in X-Ray and Gamma-Ray Instrumentation for Astronomy XIII, eds. K. A. Flanagan, & O. H. W. Siegmund, Proc. SPIE, 5165, 217
in't Zand, J. J. M. 2005, A&A, 441, L1
Kalberla, P. M. W., Burton, W. B., Hartmann, D., et al. 2005, A&A, 440, 775
Kaur, R., Heinke, C., Kotulla, R., et al. 2011, ATel, 3695
King, A. R., & Wijnands, R. 2006, MNRAS, 366, L31
Kraft, R. P., Burrows, D. N., & Nousek, J. A. 1991, ApJ, 374, 344
Kretschmar, P., Mereghetti, S., Hermsen, W., et al. 2004, ATel, 345
Krivonos, R., Revnivtsev, M., Tsygankov, S., et al. 2010, A&A, 519, A107
Lang, K. R. 1992, Astrophysical Data I. Planets and Stars., 33
Lasota, J.-P. 2001, New Astron. Rev., 45, 449
Leitch, E. M., & Vasisht, G. 1998, New Astron., 3, 51
Lin, D., Webb, N. A., & Barret, D. 2012, ApJ, 756, 27
Lutovinov, A. A., Revnivtsev, M. G., Tsygankov, S. S., & Krivonos, R. A. 2013, MNRAS, 431, 327
McClintock, J. E., & Remillard, R. A. 2006, Black hole binaries, eds. W. H. G. Lewin, & M. van der Klis, 157
Negueruela, I., Smith, D. M., Harrison, T. E., & Torrejón, J. M. 2006, ApJ, 638, 982

Negueruela, I., Torrejón, J. M., Reig, P., Ribó, M., & Smith, D. M. 2008, in A Population Explosion: The Nature and Evolution of X-ray Binaries in Diverse Environments, eds. R. M. Bandyopadhyay, S. Wachter, D. Gelino, & C. R. Gelino, AIP Conf. Ser., 1010, 252
Paizis, A., & Sidoli, L. 2014, MNRAS, 439, 3439
Paizis, A., Farinelli, R., Titarchuk, L., et al. 2006, A&A, 459, 187
Ponti, G., De Marco, B., Morris, M. R., et al. 2015a, MNRAS, 454, 1525
Ponti, G., Morris, M. R., Terrier, R., et al. 2015b, MNRAS, 453, 172
Predehl, P., & Schmitt, J. H. M. M. 1995, A&A, 293, 889
Revnivtsev, M. G., Sunyaev, R. A., Varshalovich, D. A., et al. 2004, Astron. Lett., 30, 382
Romano, P. 2015, J. High Energy Astrophys., 7, 126
Romano, P., Campana, S., Chincarini, G., et al. 2006, A&A, 456, 917
Romano, P., Barthelmy, S. D., Krimm, H. A., et al. 2011a, ATel, 3685, 1
Romano, P., Mangano, V., Cusumano, G., et al. 2011b, MNRAS, 412, L30
Romano, P., Vercellone, S., Krimm, H. A., et al. 2011c, in Proc. the 2011 Fermi Symposium, Online at http://www.slac.stanford.edu/econf/C110509/, ArXiv e-prints [arXiv:1111.0698]
Romano, P., Mangano, V., Ducci, L., et al. 2013, Adv. Space Res., 52, 1593
Romano, P., Ducci, L., Mangano, V., et al. 2014a, A&A, 568, A55
Romano, P., Krimm, H. A., Palmer, D. M., et al. 2014b, A&A, 562, A2
Romano, P., Bozzo, E., Mangano, V., et al. 2015, A&A, 576, L4
Roming, P. W. A., Kennedy, T. E., Mason, K. O., et al. 2005, Space Sci. Rev., 120, 95
Sazonov, S., Revnivtsev, M., Gilfanov, M., Churazov, E., & Sunyaev, R. 2006, A&A, 450, 117
Segreto, A., Cusumano, G., La Parola, V., et al. 2008, in Proc. 7th INTEGRAL Workshop, 131
Segreto, A., Cusumano, G., Ferrigno, C., et al. 2010a, A&A, 510, A47
Segreto, A., Cusumano, G., & La Parola, V. 2010b, in Eighth Integral Workshop. The Restless Gamma-ray Universe (INTEGRAL 2010), 71
Sguera, V., Barlow, E. J., Bird, A. J., et al. 2005, A&A, 444, 221
Sguera, V., Bazzano, A., Bird, A. J., et al. 2006, ApJ, 646, 452
Shakura, N., Postnov, K., Sidoli, L., & Paizis, A. 2014, MNRAS, 442, 2325
Sidoli, L., Belloni, T., & Mereghetti, S. 2001, A&A, 368, 835
Sidoli, L., Esposito, P., & Ducci, L. 2010, MNRAS, 409, 611
Skrutskie, M. F., Cutri, R. M., Stiening, R., et al. 2006, AJ, 131, 1163
Strüder, L., Briel, U., Dennerl, K., et al. 2001, A&A, 365, L18
Tomsick, J. A., Chaty, S., Rodriguez, J., Walter, R., & Kaaret, P. 2008, ApJ, 685, 1143
Turner, M. J. L., Abbey, A., Arnaud, M., et al. 2001, A&A, 365, L27
Ubertini, P., Lebrun, F., Di Cocco, G., et al. 2003, A&A, 411, L131
van den Heuvel, E. P. J. 2012, in Electromagnetic Radiation from Pulsars and Magnetars, eds. W. Lewandowski, O. Maron, & J. Kijak, ASP Conf. Ser., 466, 275
Vaughan, S., Goad, M. R., Beardmore, A. P., et al. 2006, ApJ, 638, 920
Walter, R., & Zurita Heras, J. 2007, A&A, 476, 335
Walter, R., Lutovinov, A. A., Bozzo, E., & Tsygankov, S. S. 2015, A&ARv, 23, 2
Watson, M. G., Schröder, A. C., Fyfe, D., et al. 2009, A&A, 493, 339
Wegner, W. 1994, MNRAS, 270, 229
White, N. E., Swank, J. H., & Holt, S. S. 1983, ApJ, 270, 711
Wijnands, R., in't Zand, J. J. M., Rupen, M., et al. 2006, A&A, 449, 1117
Wijnands, R., Degenaar, N., Armas Padilla, M., et al. 2015, MNRAS, 454, 1371